CARBON 47 (2009) 744–751

available at www.sciencedirect.com

ScienceDirect

journal homepage: www.elsevier.com/locate/carbon

Structural evolution in the graphitization process of activated carbon by high-pressure sintering

*Jinggeng Zhao, Liuxiang Yang, Fengying Li, Richeng Yu, Changqing Jin**

Beijing National Lab for Condensed Matter Physics, Institute of Physics, Chinese Academy of Sciences, Beijing 100190, PR China

ARTICLE INFO

Article history:
Received 16 July 2008
Accepted 9 November 2008
Available online 17 November 2008

ABSTRACT

Activated carbon was treated at 5 GPa up to 1600 °C, and the structural evolution in the graphitization process was investigated. The graphitization temperature is equal to 1200 °C at 5 GPa, reflected by X-ray diffraction (XRD) patterns. Honeycomb-like structures in micron scale come into being in the high-pressure sintering temperature range of 1000–1100 °C and slice-like structures appear after graphitization. The existence of D and D' lines in the Raman spectra for the graphitized-activated carbon indicates that there are still some disordered structures. The continuous occurrence of variable-range hopping, the approximately linear ρ–T relationship, and semimetal conduction mechanism accords with the graphitization process.

1. Introduction

Carbon has attracted more and more attention in scientific aspects and technological applications due to the diversity of structural and electrical properties. The forms of carbon include not only the crystalline phase of graphite, diamond and fullerene, but also many amorphous materials [1]. Recently, several interesting phenomena on carbon-based materials have been found: ferromagnetism and superconductivity fluctuation in pure highly oriented pyrolytic graphite [2,3], superconductivity in electron-doped C_{60} [4], ferromagnetism in rhombohedral C_{60} treated under high pressure and high temperature [5], complex magnetic behavior and high-pressure effect on structural and electrical properties in glassy carbon [6–8], etc. It is indicated that the ferromagnetic and superconducting properties could be ascribed to structural instability, supported by the theoretical studies [9,10]. Here, it is noted that pressure plays a significant role in treating these carbon-based materials or tuning their properties.

As one of non-crystalline carbon, the activated carbon could be used as adsorption material and catalyst due to its porosity and surface chemistry activity [11]. The radial distribution is an important method in the structural analysis of activated carbons and disordered carbons by using X-ray diffraction and neutron scattering techniques, which can provide the details of structure, including the disordered and defective features [12–17]. Activated carbon is composed of micrographites in nanometer scale with short-range order [1]. The micrographite is formed with the stack of nano-sized graphitic sheets. So the study for activated carbon is helpful to understand the properties of nano-sized materials. There may be the magnetic ordering arrangement in the zigzag edge of graphitic sheets and micrographites that are made of several sheets [18,19]. The sheets and micrographites have other special properties in electronic transportation, optical spectra, field emission, etc. [20–22]. So activated carbon should have novel properties due to its special structure.

Activated carbon can transform to graphite at high temperature, like most amorphous carbon materials [23]. The graphitization temperature of activated carbon would reach above 2500 °C at ambient condition [24]. High pressure can significantly reduce the graphitization temperature and substantially accelerate the kinetics of transformation of activated carbon and other non-crystalline carbon [25]. Inagaki

* *Corresponding author:* Fax: +86 10 82640223.
E-mail address: zhaojinggeng@163.com (C. Jin).
0008-6223/$ - see front matter
doi:10.1016/j.carbon.2008.11.006

et al. have reported that non-graphitized carbon could transform to graphite at 1500–1700 °C and 0.5 GPa [26,27]. High pressure could confine the micrographites of activated carbon in a fixed small space, while high-temperature diffusion could have them connect to each other, which accelerates the transition from activated carbon to graphite. The connections include the joint of graphitic sheets along the *c*-axis with Van der Waals force between graphitic sheets and the joint of sheets in the *ab*-plane with covalent bond between carbon atoms. Some oxide catalysts could also reduce the graphitization temperature of activated carbon [28]. The current-induced movement of Fe particles could transform the amorphous carbon nanowires into the graphitized carbon nanowires [29]. However, these methods will bring some impurity, which affects the purity of samples. Activated carbon treated under high pressure and high temperature would be pure and useful for further research and application.

In this paper, we have treated activated carbon powder by using high-pressure sintering, and researched the structural evolution in the graphitization process with X-ray diffraction (XRD) patterns, scanning electron microscope (SEM) photographs, Raman spectra, and electrical resistivity measurement.

2. Experimental

2.1. High-pressure sintering

The activated carbon produced for this work was commercial product (Beijing Chemical Reagents Company). A conventional cubic-anvil type high-pressure facility was used to perform the high-pressure and high-temperature treatments on activated carbon. The raw material, wrapped with a columned platinum foil of 5.0 mm in diameter to avoid contamination, was put into an h-BN sleeve which was in turn inserted into a graphite tube heater. Pyrophyllite was used as the pressure-transmitting medium, which can generate a fine quasi-hydrostatic environment. The treating process was carried out at 3–5 GPa and 100–1600 °C for 5–10 min, where the rate of loading pressure is about 0.3 GPa/min below 1 GPa and about 0.8 GPa/min above 1 GPa, and the rate of raising temperature is about 100 °C/min. This was followed by a quench from high temperature before releasing the pressure with the rate about 0.6 GPa/min. When the high-pressure sintering temperature is above 400 °C, the products were black and hard bulk. Here, the samples are represented as HPHT*n*, where *n* is equal to the high-pressure sintering temperature. For example, the HPHT1600 denotes activated carbon treated at 5 GPa and 1600 °C.

2.2. Sample characterization

The structures of these samples were checked by the powder XRD technology with Cu Kα radiation at room temperature, using a Rigaku diffractometer (MXP-AHP18) for $2\theta = 10–90°$. The morphologies were observed through SEM photographs on a Hitachi S-4200. Raman spectra were collected through a micro-Raman spectrometer (Jobin Yvon T64000), by using Verdi-2 solid-state laser (532 nm) as the source for excitation, with the instrument resolution 1 cm^{-1}. The measurements of temperature dependences of electrical resistivity were performed by using the standard four-probe method with Ag paste contacts on an Oxford Maglab measuring system.

3. Results and discussion

3.1. Structural property

The graphitization process of activated carbon under high pressure and high temperature can be reflected by X-ray diffraction patterns, as shown in Fig. 1a. According to the peak

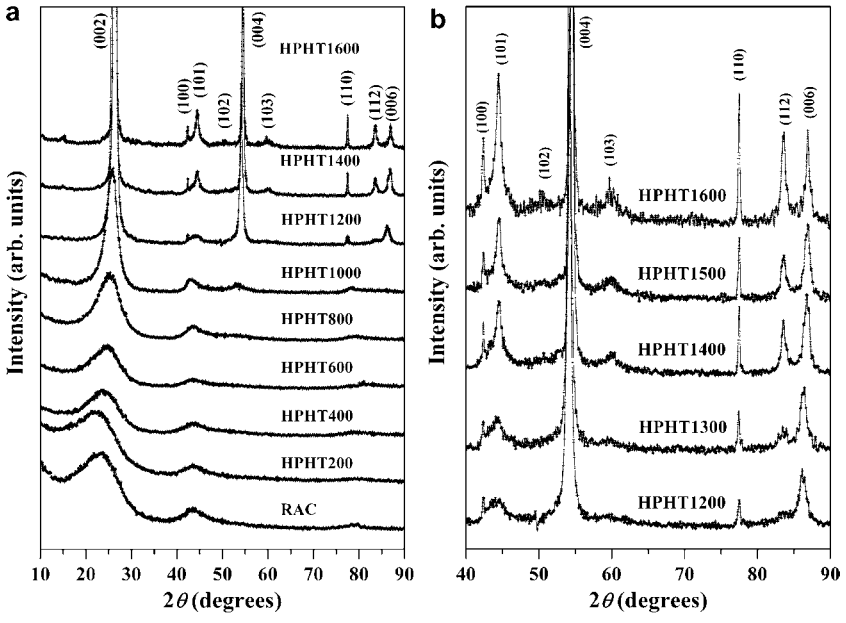

Fig. 1 – XRD patterns for (a) activated carbon prepared at 5.0 GPa and different temperatures, and (b) the graphitized-activated carbon in the range of 40–90°. The RAC represents the raw-activated carbon.

intensity evolution, the graphitization process can be distinctly viewed into three regions. The non-graphitization region, near-graphitization region, and graphitization region correspond to activated carbon treated below 900 °C, at 1000–1100 °C, and above 1200 °C, respectively. There are only the peak (*hk*) and (002) in the XRD pattern of the raw-activated carbon, being lack of other (*hkl*) peaks of graphite. When the high-pressure sintering temperature is below 1000 °C, activated carbon is non-crystalline. With increasing high-pressure sintering temperature, the (*hkl*)-type peaks come forth gradually. For the samples in the near-graphitization region, the appearance of peak (004) indicates that the graphite phase begins to come into being, but the other peaks of graphite are still not found. Activated carbon transforms to graphite at 1200 °C, while the peak (101) and (006) begin to appear and the peak (002) and (004) become very sharp. In this experiment, the graphitization temperature of activated carbon is lower than the previous results [24,26,27]. After graphitization, the (*hkl*)-type peak (102), (103) and (112) appear, with the detailed XRD patterns in the range of 40–90° shown in Fig. 1b.

Fig. 2a shows the XRD patterns of activated carbon treated at 1200 °C and, 3 and 5 GPa for 10 min, in order to research the effect of pressure on the graphitization process. At 3 GPa and 1200 °C, activated carbon can also transform to graphite. However, the graphitization degree is less than that at 5 GPa and the same sintering temperature, which indicates that the higher pressure can promote the graphitization process of activated carbon. The pressing time also is an important factor in the graphitization. So we treated activated carbon at 1200 °C and 5 GPa for different time, as shown in Fig. 2b.

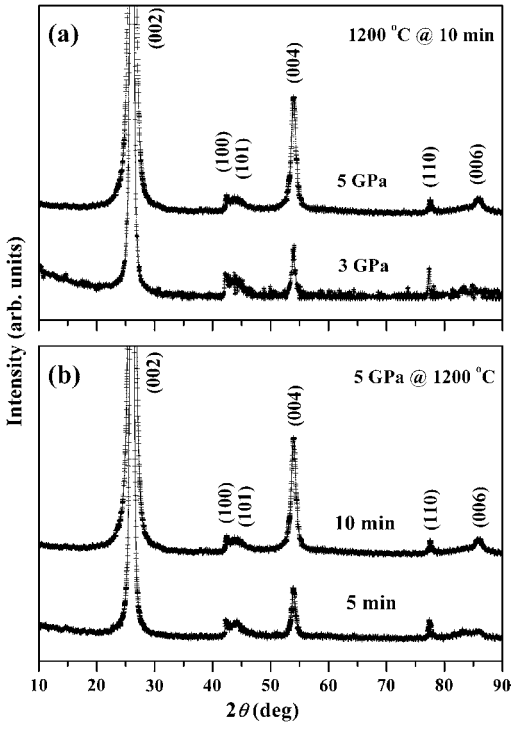

Fig. 2 – XRD patterns for the activated carbon treated (a) at 1200 °C and different pressures for 10 min, and (b) at 5 GPa and 1200 °C for different pressing time.

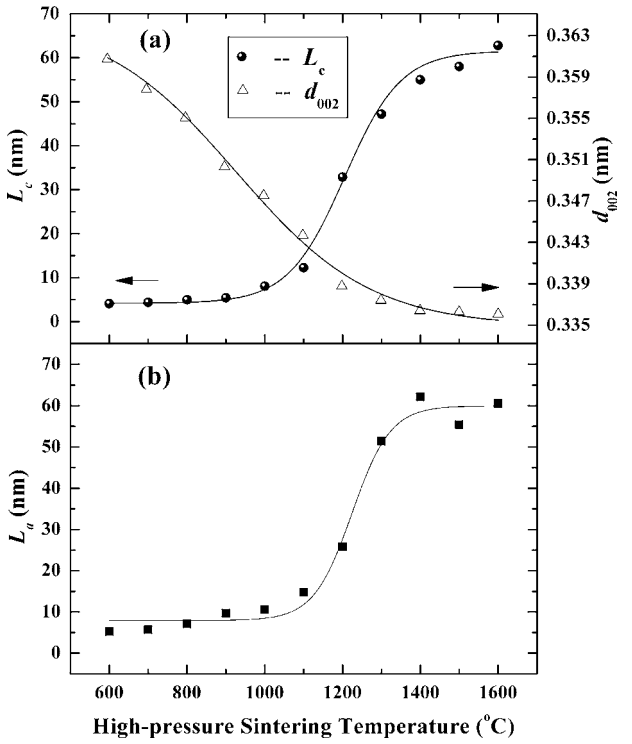

Fig. 3 – High-pressure sintering temperature dependences of (a) the *c*-axis correlation length L_c and *d* spacing of peak (002) and (b) the *a*-axis correlation length L_a for activated carbon. The black bold lines are the Boltzmann fits to these data.

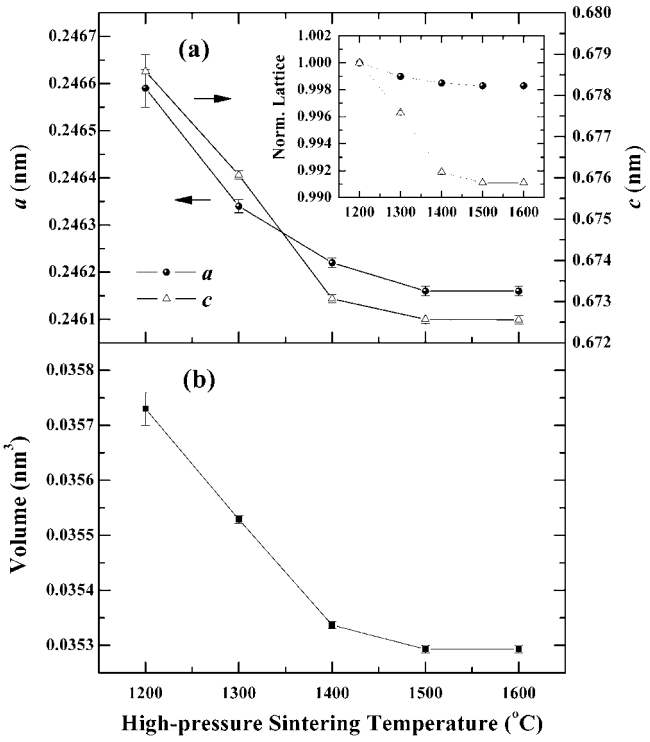

Fig. 4 – Relationships of (a) lattice parameters and (b) unit cell volume versus the high-pressure sintering temperature for the graphitized-activated carbon. The inset shows the sintering temperature dependences of normalized lattice parameters.

At the pressing time of 5 min, the graphitization of activated carbon has already finished but with a weaker crystallization compared with that at 10 min. So the longer pressing time can also enhance the graphitization degree. According to the abovementioned discussion, the graphitization degree of activated carbon can be enhanced by higher pressure and longer pressing time.

The c-axis correlation length L_c and d_{002} of HPHT600–1600 are calculated from the peak (002) by using the formula [30]

$$L_c = \frac{0.45\lambda}{\Delta \sin\theta}, \quad (1)$$

$$d_{002} = \frac{\lambda}{2\sin\theta}, \quad (2)$$

where λ is the wave length of incident X-ray, Δ is the half-width, and θ is the diffraction angle. The a-axis correlation length L_a of HPHT600–1600 is calculated from the peak (10) by using the formula [30]

$$L_a = \frac{0.92\lambda}{\Delta \sin\theta}. \quad (3)$$

The relationships of d_{002}, L_c and L_a versus high-pressure sintering temperature are shown in Fig. 3, and the data are fitted using Boltzmann function. With increasing high-pressure sintering temperature, L_c and L_a are increasing and d_{002} is decreasing. There is a drastic increase of L_c and L_a in the range of 1100–1300 °C, corresponding to the transition from near-graphitization region to graphitization region. The decrease of d value in higher high-pressure sintering temperature indicates that graphitic layers connect to each other more closely.

The lattice parameters of graphitization-activated carbon at different high-pressure sintering temperatures are calculated through the XRD patterns, with the results shown in Fig. 4a. Both the a- and c-axis shrink with increasing sintering temperature below 1500 °C, and the values of HPHT1600 are approximately equal to those of HPHT1500, which indicates that the graphitization process basically finishes at about 1500 °C. The inset of Fig. 4a shows the relationships of normalized lattice parameters versus high-pressure sintering temperature. The decrease of c-axis with sintering tempera-

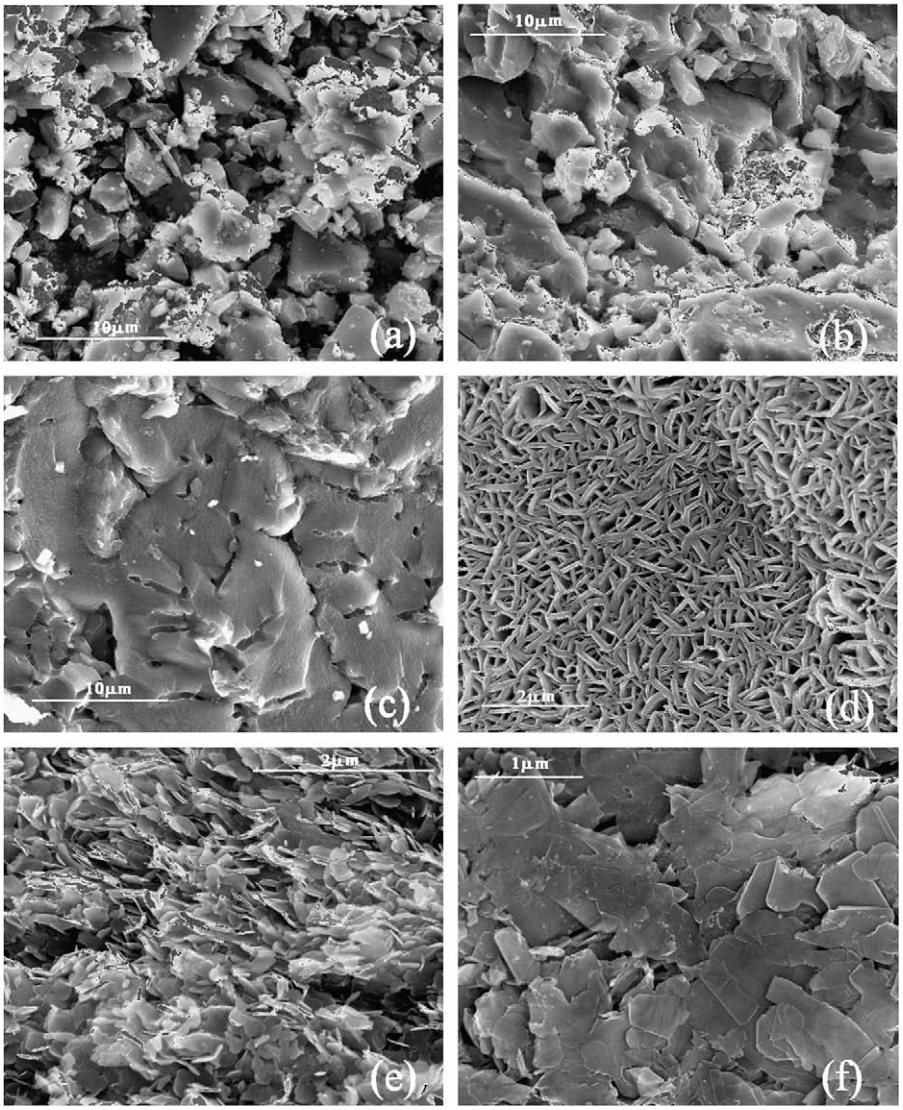

Fig. 5 – SEM photographs of (a) the raw material and activated carbon treated at (b) 700 °C, (c) 900 °C, (d) 1100 °C, (e) 1200 °C, and (f) 1600 °C.

ture is larger than that of *a*-axis, due to the weak Van der Waals force between the two neighboring layers along the *c*-axis. Fig. 4b shows the sintering temperature dependence of unit cell volume for graphitization-activated carbon. With increasing sintering temperature, the volume adopts the similar change process with that of lattice parameters.

3.2. Morphology examination by SEM

In the graphitization process of activated carbon, the morphology evolution with increasing high-pressure sintering temperature is observed using the SEM photographs. The raw-activated carbon is made of anomalistic carbon grains with size about several microns, as shown in Fig. 5a. The diameter of holes is equal to 1–6 μm, obtained from the SEM photograph, which is close to that of carbon grains. When the high-pressure sintering temperature is below 600 °C, activated carbon is still made of small grains. The carbon grains become larger with increasing high-pressure sintering temperature and begin to merge together at 700 °C, as shown in Fig. 5b. The SEM photograph of HPHT900 in Fig. 5c exhibits the high-extent merged grains. The merged grains could be reflected by the acuity of the peak (002) in XRD patterns.

For HPHT1000 and HPHT1100, the appearance of honeycomb-like structure shows the drastic change in the texture, with the result of HPHT1100 shown in Fig. 5d. These results could be corresponding to the appearance of peak (004) in XRD patterns. The micrograph indicates that the higher sintering temperature strengthens the combination among carbon grains. The interior micrographites connect each other more closely at higher high-pressure sintering temperature. However, the change of density is not obvious, as calculated from d_{002} through the formula [31]

$$\delta_{\text{X-ray}} = \frac{ZAm_H}{a_c^2 c\sqrt{3}/2} = \frac{7.627}{d_{002}}, \quad (4)$$

where $Z = 4$ is the number of carbon atoms in a unit cell, $A = 12$ is the atomic weight of carbon, $m_H = 1.66 \times 10^{-24}$ g is the mass of a hydrogen atom, and $a_c = 0.2456$ nm is the lattice constant of graphite. In other words, there is only little volume change for activated carbon from non-graphitization region to near-graphitization region. The micron scale graphite-like ribbons and holes constitute the near-graphitization activated carbon. The combination among carbon grains enlarges the holes, which results in that the sample is asymmetric in the micron scale. Comparing with graphite, it is more difficult to compress the material made of graphite-like ribbons due to its larger bulk modulus [7], and the holes remain in the sample under high pressure and high temperature. So there is the perforated structure in HPHT1000 and HPHT1100.

When the high-pressure sintering temperature is larger than 1200 °C, slice-like structures begin to form, with the micrographs of HPHT1200 and HPHT1600 shown in Fig. 5e and f, respectively. The average thickness of tens of nanometer for these slices is approximately equal to the *c*-axis correlation length L_c and the *a*-axis correlation length L_a. With increasing high-pressure sintering temperature, both the area and thickness of the slices are increasing after graphitization, which indicates that these graphitic slices become larger.

3.3. Raman spectral analysis

Fig. 6 shows the Raman spectra of activated carbon treated at different high-pressure sintering temperatures. The solid

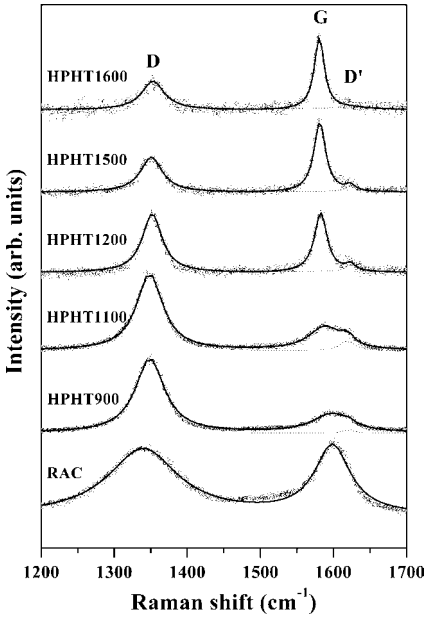

Fig. 6 – First-order Raman spectra for the raw material and activated carbon treated at 5.0 GPa and various temperatures. The solid line is the Lorentzian fit to these data, and the dashed line is the fit to the ~1620 cm^{-1} lines.

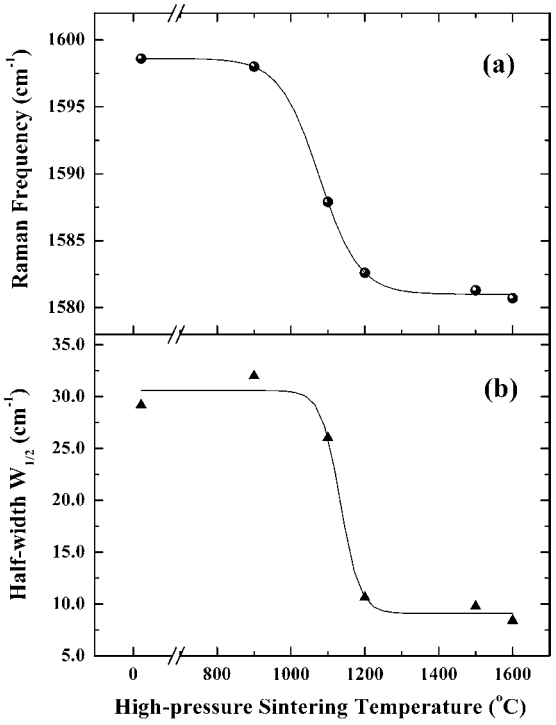

Fig. 7 – Relationships of (a) Raman frequency and (b) half-width for the dominant peak near 1580 cm^{-1} versus the high-pressure sintering temperature. The black bold lines are the Boltzmann fits to these data.

and dashed lines represent the Lorentzian fit to the whole experimental data and the results near 1620 cm^{-1}, respectively. We could observe that there are two main first-order Raman modes at ~1580 cm^{-1} and ~1350 cm^{-1}. The 1580 cm^{-1} mode (G line) corresponds to the Raman-allowed E_{2g} mode in the ideal graphite, and the 1350 cm^{-1} mode (D line) corresponds to the disorder-induced line, which associates with the large density of phonon states. The weak 1620 cm^{-1} mode (D' line) is also induced by disorder but associates with the density of mid zone phonon states [32]. Before graphitization, the intensity of G line in the Raman spectra is weak and that of D line is strong, so there are a few crystals in these samples, which could be checked by XRD patterns and SEM photographs. Raman spectroscopy could effectively reflect the degree of stacking order in graphite [33]. After graphitization, the intensity of G line begins to strengthen, but that of D line is still strong, which indicates that there are also disordered structures, being similar to the result in [34]. It should be emphasized that the spot diameter of the focused laser beam is about 1 μm, so the sample in this range contains a lot of graphitic slices, even in the graphitized-activated carbon, indicated by the SEM photographs. The edges of graphitic slices, including both armchair and zigzag edges, result in the formation of D and D' modes [35]. In our samples, the arrangement of edges in the range of laser beam is disordered, which leads to D and D' lines in the Raman spectra.

With increasing high-pressure sintering temperature, G line moves to the low-frequency direction. The relationships of Raman frequency and half-width for the G line versus high-pressure sintering temperature are shown in Fig. 7, where the black solid lines are the Boltzmann fit to these data. The frequency of 1582.6 cm^{-1} and half-width of 10.6 cm^{-1} for the G line of HPHT1200 are close to those of ideal highly oriented pyrolytic graphite [36,37]. With increasing high-pressure sintering temperature, both the frequency and half-width are decreasing and drop drastically between 1000 and 1200 °C, which corresponds to the graphitized phase transition of activated carbon.

3.4. *Electrical properties*

Fig. 8 shows the temperature dependences of electrical resistivity for activated carbon treated (a) below 800 °C, (b) at 900–1000 °C, and (c) above 1200 °C. The one-dimensional variable-range hopping conduction mechanism exists in HPHT300–800 that is made of dispersive or merged carbon grains. For HPHT900, the three-dimensional variable-range hopping is the main conduction mechanism. The relationships of resistivity versus temperature for HPHT300–900 follow the law

$$\rho(T) = \rho_0 \exp[(T_0/T)^{1/d}], \quad (5)$$

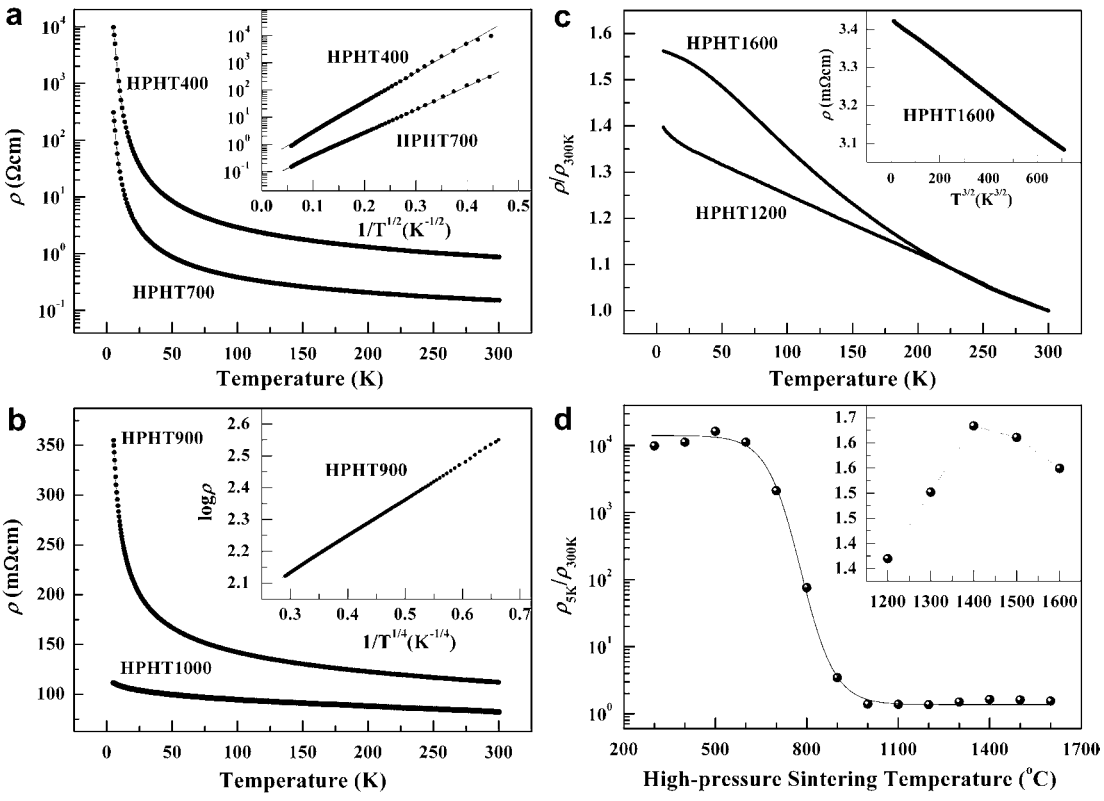

Fig. 8 – Temperature dependences of electrical resistivity for activated carbon treated (a) below 800 °C, (b) at 900–1100 °C, and (c) above 1200 °C. The insets of (a), (b), and (c) show the relationships of electrical resistivity versus $T^{-1/2}$ for HPHT400 and HPHT700, $T^{-1/4}$ for HPHT900, and $T^{3/2}$ for HPHT1600, respectively. (d) Shows the high-pressure sintering temperature dependence of the ratio of resistivity at 5 and 300 K for HPHT300–1600. The black bold line is the Boltzmann fit to these data. The inset shows the details for the graphitized-activated carbon.

where ρ_0 is the resistivity at $T = \infty$. The d is equal to 2 and 4 for HPHT300–800 and HPHT900, respectively. The insets of Fig. 8a and b show the linear relationships of $\log\rho$ versus $T^{-1/d}$. In the near-graphitization region, the relationship of electrical resistivity versus temperature is nearly linear above about 100 K, with the result of HPHT1000 shown in Fig. 8b. The conduction mechanism is intervenient the semiconductor and semimetal. According to the appearance of honeycomb-like textures in the SEM photographs, the structure of activated carbon changes dramatically and micrographites connect to each other more closely, which weakens the variable-range hopping conduction mechanism and strengthens the semimetal property of samples.

The linear relationships of resistivity versus temperature indicate that HPHT1200 and HPHT1300 have a semimetal property similar to that of a polycrystalline graphite. However, HPHT1400–1600 exhibits special electrical property and their temperature dependences of resistivity below 80 K follow the law

$$\rho(T) = \rho_0 + AT^{3/2}, \quad (6)$$

where ρ_0 is the resistivity at $T = 0$ and A is a negative constant. The inset of Fig. 8c shows the linear relationships of resistivity versus $T^{3/2}$ for HPHT1600. This non-Fermi-liquid behavior is attributed to the disordered structures in the graphitized-activated carbon, reflected by the SEM photographs and Raman spectra.

Fig. 8d shows the relationship of $\rho_{5\ K}/\rho_{300\ K}$ versus high-pressure sintering temperature for HPHT300–1600. The black bold line is Boltzmann fit to these data. The inset shows the details in the range of 1200–1600 °C. The ratio decreases drastically between 700 and 1000 °C. The insulator–metal transition occurs in the range of 900–1000 °C, which is less than that of activated carbon treated only at high temperature [38].

4. Conclusions

We treated activated carbon at 5 GPa up to 1600 °C and found that high pressure can accelerate its graphitization process, with the graphitization temperature as low as 1200 °C, indicated by XRD patterns. With increasing high-pressure sintering temperature, the texture of activated carbon changes from dispersive or merged carbon grains in the non-graphitization region across honeycomb-like structures in the near-graphitization region to slice-like structures after graphitization. Raman frequency and half-width of G line in the graphitized-activated carbon are close to those of highly oriented pyrolytic graphite, but there are still some disordered structures in these samples. The electrical property transition corresponds to the structural evolution in the graphitization process very well. The insulator–metal transition occurs between non-graphitization region and near-graphitization region.

Acknowledgements

We thank Prof. C. Dong and H. Chen of Institute of Physics, Chinese Academy of Sciences for their help in XRD measurement and analysis, and the support from NSF and Ministry of Science and Technology of China through the research projects.

REFERENCES

[1] Robertson J. Amorphous-carbon. Adv Phys 1986;35(4):317–74.
[2] Kopelevich Y, Esquinazi P, Torres JHS, Moehlecke S. Ferromagnetic- and superconducting-like behavior of graphite. J Low Temp Phys 2000;119(5–6):691–702.
[3] Kempa H, Kopelevich Y, Mrowka F, Setzer A, Torres JHS, Höhne R, et al. Magnetic-field-driven superconductor–insulator-type transition in graphite. Solid State Commun 2000;115(10):539–42.
[4] Hebard AF, Rosseinsky MJ, Haddon RC, Murphy DW, Glarum SJ, Palstra TTM, et al. Superconductivity at 18-K in potassium-doped C-60. Nature 1991;350(6319):600–1.
[5] Makarova TL, Sundquist B, Höhne R, Esquinazi P, Kopelevich Y, Scharff P, et al. Magnetic carbon. Nature 2001;413(6857):716–8.
[6] Wang X, Liu ZX, Zhang YL, Li FY, Yu RC, Jin CQ. Evolution of magnetic behaviour in the graphitization process of glassy carbon. J Phys Condens Matter 2002;14(43):10265–72.
[7] Wang X, Bao ZX, Zhang YL, Li FY, Yu RC, Jin CQ. High pressure effect on structural and electrical properties of glassy carbon. J Appl Phys 2003;93(4):1991–4.
[8] Jin CQ, Wang X, Liu ZX, Zhang YL, Li FY, Yu RC. The unusual morphology, structure, and magnetic property evolution of glassy carbon upon high pressure treatment. Braz J Phys 2003;33(4):723–8.
[9] González J, Guinea F, Vozmediano MAH. Electron–electron interactions in graphene sheets. Phys Rev B 2000;63(13):134421.
[10] Harigaya K. The mechanism of magnetism in stacked nanographite: theoretical study. J Phys Condens Matter 2001;13(6):1295–302.
[11] Jordá-Beneyto M, Suárez-García F, Lozano-Castelló D, Cazorla-Amorós D, Linares-Solano A. Hydrogen storage on chemically activated carbons and carbon nanomaterials at high pressures. Carbon 2007;45(2):293–303.
[12] Burian A, Dore JC, Hannon AC, Honkimaki V. Complementary studies of structural characteristics for carbon materials with X-rays and neutrons. J Alloy Compd 2005;401(1–2):18–23.
[13] Burian A, Ratuszna A, Dore JC, Howells SW. Radial distribution function analysis of the structure of activated carbons. Carbon 1998;36(11):1613–21.
[14] Dore JC, Sliwinski M, Burian A, Howells WS, Cazorla D. Structural studies of activated carbons by pulsed neutron diffraction. J Phys Condens Matter 1999;11(47):9189–201.
[15] Szczygielska A, Burian A, Dore JC. Paracrystalline structure of activated carbons. J Phys Condens Matter 2001;13(24):5545–61.
[16] Burian A, Dore JC, Kyotani T, Honkimaki V. Structural studies of oriented carbon nanotubes in alumina channels using high energy X-ray diffraction. Carbon 2005;43(13):2723–9.
[17] Burian A, Brodka A, Koloczek J, Dore JC, Hannon AC, Fonseca A. Energy relaxation and pulsed neutrons diffraction studies of carbon nanotubes. Diamond Relat Mater 2006;15(4–8):1090–3.
[18] Fujita M, Wakabayashi K, Nakada K. Peculiar localized state at zigzag graphite edge. J Phys Soc Jpn 1996;65(7):1920–3.
[19] Nakada K, Fujita M. Edge state in graphene ribbons: nanometer size effect and edge shape dependence. Phys Rev B 1996;54(24):17954–61.
[20] Nakada K, Igami M, Fujita M. Electron–electron interaction in nanographite ribbons. J Phys Soc Jpn 1998;67(7):2388–94.
[21] Wakabayashi K, Fujita M, Ajiki H, Sigrist M. Electronic and magnetic properties of nanographite ribbons. Phys Rev B 1999;59(12):8271–82.

[22] Chiu CW, Shyu FL, Chang CP, Chen RB, Lin MF. Optical spectra of AB- and AA-stacked nanographite ribbons. J Phys Soc Jpn 2003;72(1):170–7.
[23] Franklin RE. Crystallite growth in graphitizing and non-graphitizing carbons. Proc Roy Soc London Ser A 1951;209:196–218.
[24] Hishiyama Y, Inagaki M, Kimura S, Yamada S. Graphitization of carbon fibre/glassy carbon composites. Carbon 1974;12(3):249–58.
[25] Wang X, Zhang GM, Zhang YL, Li FY, Yu RC, Jin CQ, et al. Graphitization of glassy carbon prepared under high temperatures and high pressures. Carbon 2003;41(1):188–91.
[26] Inagaki M, Oberlin A, de Fonton S. Texture change in hard carbon on heat treatment under pressure. High Temp High Press 1977;9(4):453–60.
[27] Inagaki M, Naka S. Crystallite orientation in polycrystalline graphites made from glass-like carbons under high-pressure. J Mater Sci 1975;10(5):814–8.
[28] Mochida I, Ohtsubo R, Takeshita K, Marsh H. Catalytic graphitization of non-graphitizable carbon by chromium and manganese oxides. Carbon 1980;18(2):117–23.
[29] Jin CH, Wang JY, Chen Q, Peng LM. In situ fabrication and graphitization of amorphous carbon nanowires and their electrical properties. J Phys Chem B 2006;110(11):5423–8.
[30] Short MA, Warlker Jr PL. Measurement of interlayer spacings and crystal sizes in turbostratic carbons. Carbon 1963;1(1):3–9.
[31] Dubinin MM, Plavnik GM, Zaverina ED. Integrated study of the porous structure of active carbons from carbonized sucrose. Carbon 1964;2(3):261–8.
[32] Nemanich RJ, Solin SA. First- and second-order Raman scattering from finite-size crystals of graphite. Phys Rev B 1979;20(2):392–401.
[33] Cancado LG, Takai K, Enoki T, Endo M, Kim YA, Mizusakim H, et al. Measuring the degree of stacking order in graphite by Raman spectroscopy. Carbon 2008;46(2):272–5.
[34] Kuriyama K, Dresselhaus MS. Metal–insulator-transition in highly disordered carbon-fibers. J Mater Res 1992;7(4):940–5.
[35] Cancado LG, Pimenta MA, Neves BRA, Dantas MSS, Jorio A. Influence of the atomic structure on the Raman spectra of graphite edges. Phys Rev Lett 2004;93(24):247401-1–4.
[36] Tuinstra F, Koenig JL. Raman spectrum of graphite. J Chem Phys 1970;53(3):1126–30.
[37] Tuinstra F, Koenig JL. Characterization of graphite fiber surfaces with Raman spectroscopy. J Compos Mater 1970;4:492–9.
[38] Fung AWP, Dresselhaus MS, Endo M. Phys Rev B 1993;48:14953–62.